THE JOURNAL OF BIOLOGICAL CHEMISTRY VOL. 284, NO. 7, pp. 4713–4722, February 13, 2009

Migfilin, a Molecular Switch in Regulation of Integrin Activation*[S]

Received for publication, October 6, 2008, and in revised form, December 1, 2008 Published, JBC Papers in Press, December 13, 2008, DOI 10.1074/jbc.M807719200

Sujay Subbayya Ithychanda[‡1], Mitali Das[‡1], Yan-Qing Ma[‡], Keyang Ding[‡], Xiaoxia Wang[‡], Sudhiranjan Gupta[‡], Chuanyue Wu[§], Edward F. Plow[‡2], and Jun Qin[‡3]

From the [‡]Department of Molecular Cardiology, Lerner Research Institute, Cleveland Clinic, Cleveland, Ohio 44195 and the [§]Department of Pathology, University of Pittsburgh, Pittsburgh, Pennsylvania 15261

The linkage of heterodimeric (α/β) integrin receptors with their extracellular matrix ligands and intracellular actin cytoskeleton is a fundamental step for controlling cell adhesion and migration.Binding of the actin-linking protein, talin, to integrin β cytoplasmic tails (CTs) induces high affinity ligand binding (integrin activation), whereas binding of another actin-linking protein, filamin, to the integrin β CTs negatively regulates this process by blocking the talin-integrin interaction. Here we show structurally that migfilin, a novel cytoskeletal adaptor highly enriched in the integrin adhesion sites, strongly interacts with the same region in filamin where integrin β CTs bind. We further demonstrate that the migfilin interaction dissociates filamin from integrin and promotes the talin/integrin binding and integrin activation. Migfilin thus acts as a molecular switch to disconnect filamin from integrin for regulating integrin activation and dynamics of extracellular matrix-actin linkage.

Cells reside in a protein network, the extracellular matrix (ECM).[4] Cell-ECM contact is crucial for many physiological and pathophysiological processes and is primarily mediated by heterodimeric (α/β) transmembrane receptors, the integrins (1). Integrins engage a variety of ECM proteins via their extracellular domains while connecting to the actin cytoskeleton via their small cytoplasmic tails (CTs). The ability of integrins to bind to their ligands is uniquely controlled by the integrin CTs via a process called "inside-out signaling," *i.e.* upon cellular stimulation, an integrin, typically expressed in a latent state, can receive intracellular signal(s) at its CT, which transmits through the transmembrane domain to the extracellular domain thereby converting the receptor from a low to a high affinity state (integrin activation). How such long range information transfer is initiated and regulated has been the central topic of integrin/cell adhesion research over the decades (for reviews see Refs. 2–5). Structural/biochemical studies have indicated that the inside-out signaling involves the unclasping of the integrin α/β CT complex (6–9), followed by extensive rearrangement of transmembrane domain and extracellular domain (10–13). Talin, a large actin-linking protein, was found to play a key role in the unclasping process by binding to the integrin β CTs (7–8, 14). Talin activity appears to be controlled by multiple factors or pathways (15–20).

Relevant to this study is the role of filamin, another major actin cross-linking protein (21–22), in integrin activation. Filamin was found to share an overlapping binding site on integrin β CTs with talin and thus suppress the talin-integrin interaction (16). Gene silencing of filamin in various cell lines to remove the filamin-integrin connection enhances integrin activation (16, 23), whereas increased filamin-integrin interaction inhibits cell migration (24), a process critically dependent on integrin activation. Together these observations support the notion that filamin binding to integrin serves as a cellular brake to control the dynamics of the integrin activation by inhibiting talin function and ECM-cytoskeleton communication. The mechanism as to how the filamin brake is turned off to promote integrin activation and cell migration is not understood.

Filamin is known to contain an N-terminal actin binding domain (ABD) and a long rod-like domain of 24 immunoglobulin-like repeats, of which repeat 21 (IgFLN21) was shown to play a key role in binding to integrin β CTs and blocking the talin-integrin β CT interaction (16). Interestingly, IgFLN21 also recognizes another intracellular protein called migfilin, which has been shown to be an important regulator of integrin-mediated cytoskeletal rearrangements, cell shape change (25), and cell migration (26).

In an effort to dissect the complex intermolecular interactions between migfilin, filamin, and integrin, we have undertaken a detailed structural/functional analysis. Using NMR spectroscopy, we have mapped the precise IgFLN21 binding region in migfilin, which is located at the extreme N terminus (residues 1–24) of migfilin (migfilin-N), and we solved solution

* This work was supported, in whole or in part, by National Institutes of Health Grants GM62823 (to J. Q.) and P01HL073311 (to J. Q. and E. F. P.). The costs of publication of this article were defrayed in part by the payment of page charges. This article must therefore be hereby marked "*advertisement*" in accordance with 18 U.S.C. Section 1734 solely to indicate this fact.

The atomic coordinates and structure factors (code 2K9U) have been deposited in the Protein Data Bank, Research Collaboratory for Structural Bioinformatics, Rutgers University, New Brunswick, NJ (http://www.rcsb.org/).

[S] The on-line version of this article (available at http://www.jbc.org) contains supplemental Figs. S1–S7.

[1] Both authors contributed equally to this work.

[2] To whom correspondence may be addressed: Dept. of Molecular Cardiology, NB20, Lerner Research Institute, Cleveland Clinic, 9500 Euclid Ave., Cleveland, OH 44195. Tel.: 216-444-5392; Fax: 216-445-1466; E-mail: plowe@ccf.org.

[3] To whom correspondence may be addressed. Tel.: 216-444-5392; Fax: 216-445-1466; E-mail: qinj@ccf.org.

[4] The abbreviations used are: ECM, extracellular matrix; CT, cytoplasmic tail; ITC, isothermal titration calorimetry; FITC, fluorescein isothiocyanate; WT, wild type; MT, mutant; NOE, nuclear Overhauser effect; FACS, fluorescence-activated cell sorter; HSQC, heteronuclear single quantum coherence; PDB, Protein Data Bank; CHO, Chinese hamster ovary; GST, glutathione *S*-transferase; mAb, monoclonal antibody; GFP, green fluorescent protein; PTB, phosphotyrosine binding.

structure of the IgFLN21-migfilin-N complex. To our surprise, despite little sequence homology, migfilin binds to the same region in IgFLN21 where integrin β CT binds. Detailed NMR and biochemical analyses demonstrate that the migfilin-filamin interaction is an order of magnitude higher than the integrin-filamin interaction and that the migfilin binding to filamin can competitively dissociate filamin from integrin and thus promote the talin-integrin interaction. Using multiple functional approaches, we further show that migfilin, but not its filamin binding defective mutant, significantly enhances integrin activation. These data suggest a novel regulatory pathway in which the binding of filamin to its downstream target migfilin switches off the integrin-filamin connection, thereby promoting talin binding to and activation of integrins.

EXPERIMENTAL PROCEDURES

Plasmid, Peptide Constructs, and Purification—Human IgFLNc21-(2282–2395) was cloned into pGEX 5X-1 (Amersham Biosciences) with glutathione *S*-transferase as fusion tag and expressed in *Escherichia coli* BL21 (DE3). Cells were induced at room temperature with 250 mM isopropyl 1-thio-β-D-galactopyranoside for 16 h when the A_{600} was 0.6. The protein was purified on glutathione-Sepharose 4B to homogeneity and cleaved with factor Xa to release the fusion partners. Rebinding of GST to the column gave a preparation consisting predominantly of IgFLNc21, which was then subjected to gel filtration to remove residual GST to yield homogeneous IgFLNc21. A five-amino acid segment remains with IgFLNc21 as a cloning artifact bringing the total length of the fragment used for structure determinations to 119 residues. To prepare ^{15}N- and/or ^{13}C-labeled protein, $^{15}NH_4Cl$ and [^{13}C]glucose were added to M9 medium. The N-terminal 85-residue filamin binding domain of migfilin (Migfilin-Nter) was cloned in pMalC2X vector and expressed in *E. coli* BL21. The *E. coli* expressed MBP-Migfilin-Nter protein was used for initial binding studies to filamin, and specific binding of migfilin to IgFLNc21 was confirmed by HSQC perturbation. Subsequent cleavage to release Migfilin-Nter was only partly successful as the protein tended to degrade on purification. GST-fused Migfilin-Nter was therefore expressed along with chaperone coexpression (Takara Bio Inc.) in *E. coli* to generate Migfilin-Nter of better quality and quantity. N-terminal migfilin peptides, 34 and 24 residues in length, and β7 peptide (see Fig. 3*A*) were synthesized by the in-house Biotechnology Core Facility. IgFLNa21-(2236–2329) was cloned in pGST-parallel vector, expressed in *E. coli* BL21 (DE3) and purified using standard protocols. GFP-tagged migfilin was generated using the pEGFP-N1 vector using the EcoRI and KpnI restriction sites.

Isothermal Titration Calorimetry (ITC)—A Microcal VP-ITC instrument was used for calorimetric studies. Proteins (IgFLNa21 and IgFLNc21) were extensively buffer-exchanged into 25 mM sodium phosphate, pH 6.4, 5 mM NaCl, and 1 mM dithiothreitol. Peptides were weighed (β7 and migfilin-N) and directly dissolved in the above buffer. Experiments were performed at 29 °C to match the NMR spectroscopy conditions. Binding was assumed to be 1:1.

NMR Spectroscopy—All NMR experiments were performed on Bruker 600-MHz spectrometer equipped with a triple resonance probe at 29 °C in 25 mM sodium phosphate, pH 6.4, 50 mM NaCl, and 1 mM dithiothreitol. Resonance assignments of IgFLNc21 with bound migfilin-N peptide were achieved with standard triple resonance experiments on a single ^{13}C-^{15}N-labeled sample with 1 mM IgFLNc21 and 2 mM migfilin-N peptide. NOE analyses were made using 120-ms mixing time for the ^{13}C-^{15}N-edited nuclear Overhauser effect spectroscopy experiments. Resonance assignments of the unlabeled 24-residue migfilin-N peptide were made using filtered total correlation spectroscopy (mixing time 70 ms) and filtered nuclear Overhauser effect spectroscopy (mixing time 150 ms) experiments. Spectra were processed by NMRPipe (27) and visualized PIPP (28). PASA software was used in the assignment of chemical shifts (29).

Structure Calculation—X-plor-NIH (30) was used for calculating structure. The structure of IgFLNc21 was calculated with intramolecular NOEs and dihedral angle restraints derived from the TALOS program (31). The complex structure was then calculated by including 130 intermolecular NOEs between IgFLNc21 and migfilin-N and intramolecular NOEs for migfilin-N. Hydrogen-deuterium exchange-based experimental hydrogen bonding constraints were also used for further refinement at the final stage of the structure calculations. Structure quality was evaluated using PROCHECK (32). The final 20 lowest energy structure coordinates are deposited in the Protein Data Bank (PDB) and assigned as code 2K9U. The complete list of constraints used for structure calculation is submitted to BMRB data base (accession number 16002).

Western Blotting—Purified platelets from 50 ml of blood were lysed in 50 mM Tris·HCl, pH 7.4, 150 mM NaCl, 1% Triton X-100, and 1 tablet of protease inhibitor (Roche Applied Science) by gentle pipetting. Lysed platelets were centrifuged at 13,000 $\times$ *g* for 5 min, and the supernatant was used for co-immunoprecipitation experiments. From this lysate, 100 μl (2 mg of protein) was diluted with 900 μl of RIPA buffer (1$\times$ Tris-buffered saline, 1% Nonidet P-40, 0.5% sodium deoxycholate, 0.1% SDS, 0.004% sodium azide) containing phenylmethylsulfonyl fluoride, protease inhibitor mixture, and sodium orthovanadate (Santa Cruz Biotechnology). The diluted lysate was precleared with protein A/G PLUS beads (Santa Cruz Biotechnology) for 45 min. The supernatant (1 ml) was incubated with 25 μl of anti-filamin antibody (Cell Signaling Technology) with mild rocking for 4 h, and 40 μl of protein A/G was added followed by overnight incubation. Amount of integrin β3 bound to filamin was estimated in the presence/absence of migfilin-N peptide in the platelet lysate by Western blotting using anti-integrin β3 antibody (BD Biosciences).

Isolation of Platelets from Human Blood—Platelets were isolated as described previously (33). Briefly, blood was drawn from healthy volunteers into acid/citrate/dextrose (ACD: 65 mM citric acid, 85 mM sodium citrate, 111 mM dextrose, pH 4.61) and 2 μM prostaglandin E_1. Blood was centrifuged to obtain platelet-rich-plasma, which was then further centrifuged, and the platelet pellet was suspended in Ca^{2+}- and Mg^{2+}-free Tyrode's buffer (138 mM NaCl, 12 mM $NaHCO_3$, 0.36 mM Na_2HPO_4, 2.9 mM KCl, 10 mM HEPES, 0.1% glucose, 0.1% bovine serum albumin, pH 7.4). This was filtered through a Sepharose CL-4B (GE Healthcare) column in Tyrode's buffer

to obtain the platelet preparations used. Platelet count was determined using an automated cell counter (Nexcelcom Bioscience). $MgCl_2$ and $CaCl_2$ in the concentrations of 1 and 2 mM, respectively, were added to the platelet suspension just before experiments, unless otherwise indicated.

A5 Cells—Chinese hamster ovary (CHO) cells stably expressing αIIbβ3 integrin (A5 cells) were detached as described (9).

Peptide Conjugation—Truncated versions of IgFLN21 binding migfilin-N wild type and mutant peptides (^{4}KPEKRVASSVFITLAP^{19}C and ^{4}KPEKRVA**D**S**A**FITLAP^{19}C), were made with an additional C-terminal cysteine residue (in boldface type). CR_7 transport peptide was activated with 2,2′-dithiobis(5-nitropyridine) and conjugated to the migfilin peptides by minor modifications of reported methods (34). The conjugated peptides were purified by high pressure liquid chromatography and conjugation confirmed by electrospray ionization mass spectrometry. Conjugated peptides were also made with a single FITC-group at the N terminus, adding the FITC group during the synthesis of the peptides.

Peptide Uptake into Platelets and A5 Cells—Peptide uptake into platelets and A5 cells was analyzed by flow cytometry (FACS) and confocal microscopy. Gel-filtered platelets (5×10^8 ml^{-1}) or A5 cells ($1–2 \times 10^6$ ml^{-1}) were incubated with 10 μM FITC-WTmigfilinCCR7, FITC-MTmigfilinCCR7, FITC-migfilin, migfilin, or CR7 peptides for 5 min at 37 °C and fixed with 0.5% (platelets) or 2% (A5 cells) paraformaldehyde in 1× phosphate-buffered saline. Samples were washed and resuspended in phosphate-buffered saline. All flow cytometry analyses were done in an LSR instrument (BD Biosciences), and data were analyzed with FlowJo software 8.7.3 (Treestar). For each sample, 100,000 platelets or 10,000 A5 cells were counted. Platelets/A5 cells were prepared similarly for confocal microscopy. Cells were analyzed using a Leica microscope using a 100× oil immersion objective for platelets and 63× lens for A5 cells.

Fibronectin or HUTS-4 Binding to A7 Cells—Melanoma cells line A7 (FLNA$^+$) was obtained from ATCC and cultured as described previously (35). Migfilin full-length subcloned into EGFP-N1 plasmid (Clontech) was used to transiently transfect A7 cells with Lipofectamine 2000 (Invitrogen). Cells were grown to 95% confluence and transfected with 2 μg of plasmid DNA. After 4 h, cells were washed, and integrin activation was assessed at 24 h.

A7 cells were detached as the A5 cells. Live cells were distinguished from dead cells by staining with LIVE/DEAD dye (Molecular Probes) (1 μl of dye per 10^6 cells), and this dye was included in all analyses with cultured cells. Cells were incubated with 30 μg ml^{-1} Alexa Fluor 647 (Molecular Probes)-labeled 120-kDa fibronectin fragment (Millipore) or 20 μg ml^{-1} of HUTS-4 monoclonal antibody (Millipore) for 30 min at 37 °C in dark. For HUTS-4 binding, cells were incubated further with 20 μg ml^{-1} of Alexa Fluor 633 anti-mouse IgG (Molecular Probes) for 30 min on ice in the dark. After fibronectin or HUTS-4 binding, washed and fixed cells were analyzed by flow cytometry. Fibronectin or HUTS-4 binding was calculated from 10,000 live GFP$^+$ cells per sample that bound fibronectin or HUTS-4 and corrected for GFP fluorescence. Intensity calibration beads for 633 or 647 nm excitation/660 nm emission (fibronectin or HUTS-4) and 488 nm excitation/515 nm emission (Molecular Probes) (GFP) were included in each experiment. Binding because of migfilin full-length is represented as fold increase over vector alone.

αIIbβ3 Activation in Platelets—PAC1, the mAb that reacts selectively with the active conformation of αIIbβ3 was used as in Ref. 36. Platelets ($7–10 \times 10^8$ ml^{-1}) were incubated with 10 μM of the respective unlabeled peptides at 37 °C for 5 min followed by 40 μg ml^{-1} FITC-PAC1 IgM for 30 min at room temperature in the dark. This was followed by addition of 500 μl of the Tyrode's buffer, pH 7.4, and immediate analysis by FACS. Data acquisition and processing were the same as for peptide uptake analyses. Specific binding was expressed in terms of median fluorescent intensities. Nonspecific binding was based on binding because of FITC-PAC1 alone. At the end of each experiment, intensity calibration beads were run as above for fibronectin/HUTS4 binding of A7 cells. The relative fluorescent intensities displayed on graphs are the median fluorescent intensities-based on the calibration beads.

PAC1 or Fibrinogen Binding of A5 Cells—50-μl aliquots of A5 cells ($1.5–2 \times 10^6$ ml^{-1}) were incubated with 10 μM of unlabeled peptides at 37 °C for 5 min, and PAC1 binding done as described (9) using Alexa Fluor 633 goat anti-mouse IgM conjugate (Molecular Probes) for detection. For some experiments, A5 cells were incubated with 125 μg ml^{-1} of Alexa Fluor 488 conjugate of fibrinogen (Molecular Probes) for 30 min at 37 °C after peptide treatment. After washing and fixation, FACS was done. Specific PAC1 or fibrinogen binding was calculated by subtracting nonspecific binding because of the Alexa Fluor 633 goat anti-mouse IgM conjugate or Alexa Fluor 488-fibrinogen alone, respectively. The relative fluorescent intensities were calculated as before.

Platelet Aggregation—Effect of FITC-labeled or -unlabeled migfilin peptides on platelet aggregation was examined using an aggregometer (Chronolog Corp.). In siliconized cuvettes, Tyrode's buffer supplemented with 2 mM $CaCl_2$ and 1 mM $MgCl_2$ and platelets ($0.5–4 \times 10^8$ ml^{-1}) were equilibrated at 37 °C for 5 min. Then 10 μM of the selected peptide or agonist was added, and aggregation was monitored for 5 min at 37 °C with stirring. The final volume in each cuvette was 500 μl. TRAP6 (10 μM concentration) was used as a positive control, and base line for 100% aggregation was set with Tyrode's buffer. Quantitation of the effects of the peptides is based by assigning TRAP6 aggregation a value of 100%.

RESULTS

Characterization of Migfilin Binding to Filamin—Migfilin (25), also known as Cal (37) or FBLP-1A (38), is a widely expressed 373-amino acid protein containing an N-terminal region, a middle proline-rich region, and three C-terminal consecutive LIM domains. Migfilin has two isoforms: migfilin(s) that lacks the proline-rich region, and FBLP-1 that lacks the third LIM domain (39). Previous functional studies have shown that the N-terminal residues 1–85 of migfilin recognize repeat 21 of filamin A or C (isoforms of 91% identity, supplemental Fig. S1) (25). Migfilin-(1–85) has no sequence homology to any known protein, and its binding mode to filamin is unknown. Fig. 1*A* shows the ^{1}H-^{15}N HSQC spectrum of filamin C repeat

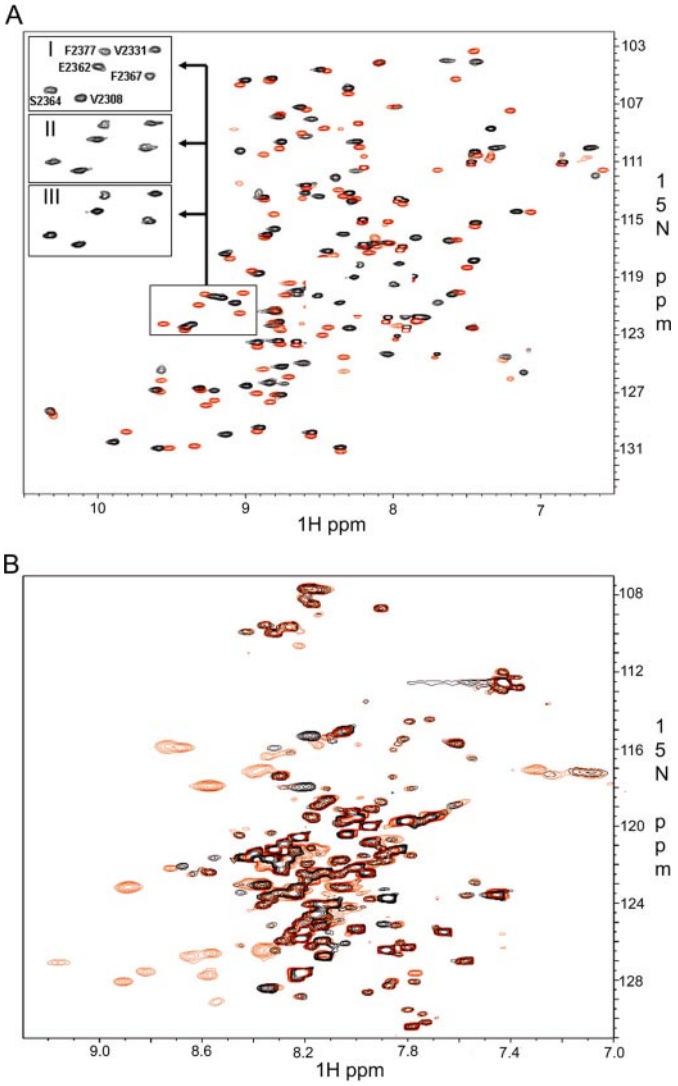

FIGURE 1. **IgFLNc21-migfilin-N interaction.** *A,* 600-MHz two-dimensional ^{1}H-^{15}N HSQC of 0.2 mM ^{15}N-labeled IgFLNc21 in the absence (*black*) and presence (*red*) of 0.4 mM unlabeled migfilin-N at pH 6.5, 29 °C. *Insets I–III* are the zoomed region of IgFLNc21 in the presence of the different migfilin fragments. *Inset I,* 1–85; *II,* 1–36; and *III,* 1–24. The spectral patterns in the insets are identical indicating that migfilin-(1–24) fragment (migfilin-N) is sufficient to bind to IgFLN21. *B,* HSQC of 0.2 mM ^{15}N-labeled migfilin-(1–85) in the absence (*black*) and presence (*red*) of 0.4 mM IgFLNc21 at identical experimental conditions, showing that IgFLNc21 induced substantial chemical shift changes of a dozen residues as consistent with the result in *A*.

21 (IgFLNc21) in the absence and presence of unlabeled migfilin-(1–85). Substantial chemical shift changes were observed for IgFLNc21 upon addition of migfilin-(1–85) suggesting strong interaction. Fig. 1*B* shows the converse HSQC spectrum, ^{15}N-labeled migfilin-(1–85), in the absence and presence of unlabeled IgFLNc21. The free form of migfilin-(1–85) appears to be intrinsically unstructured as indicated by its very narrow spectral dispersion. However, upon binding to IgFLNc21, 12 residues in migfilin-(1–85) underwent dramatic chemical shift changes, whereas the majority of the signals remained unperturbed, indicating that only a small portion of migfilin is involved in binding to IgFLNc21, but this portion appears to be changed dramatically by the interaction. To map the precise filamin binding region in migfilin-(1–85), we synthesized two deletion mutants, truncating the C terminus of migfilin-(1–85) to generate migfilin-(1–36) and migfilin-(1–24). Fig. 1*A* shows that these deletion mutants induced identical chemical shift changes in IgFLN21 compared with migfilin-(1–85), demonstrating that the first 24 residues of migfilin are sufficient for binding to IgFLNc21. This is consistent with the previous cell-based analysis in which deletion of migfilin-(1–24) (migfilin-N) completely abolished the migfilin binding to filamin and impaired actin assembly (25). During all the above HSQC titrations, no appreciable increase in line widths was observed. Many residues that could not be assigned with the free form of filamin appeared sharper indicating better structuring of the repeat, thereby negating any appreciable dimer formation on migfilin binding. Filamin A repeat 21 (IgFLNa21) also interacted with migfilin-N in a similar manner (see supplemental Fig. S2) with essentially the same affinity (K_d ~2.5 μM) as IgFLNc21 (K_d ~2.4 μM), as shown by ITC experiments (Fig. 2). Interestingly, migfilin-N induced a quite distinct spectral pattern in IgFLN21 as compared with integrin β7 CT (supplemental Fig. S2), which is the highest affinity integrin β CT binding partner of IgFLN21 (16). Overall, more significant chemical shift changes of IgFLN21 occurred upon binding to migfilin-N than to β7 CT, suggesting that the filamin-migfilin interaction is stronger than the filamin-integrin interaction. To confirm this, we performed the ITC experiments, which revealed that the affinity of migfilin-N/IgFLNa21 was an order of magnitude higher than that for integrin β7/IgFLNa21 (Fig. 2).

NMR Structure of IgFLN21 in Complex with Migfilin-N Reveals That Migfilin and Integrin β CTs Share an Overlapping Binding Site on IgFLN21—Recent crystallographic data have resolved how IgFLNa21 and integrin β CTs interact (16). However, sequence comparison between integrin β CTs and migfilin-N revealed that, although integrin β CTs are highly homologous to one another, they are quite dissimilar from migfilin-N (Fig. 3*A*) leaving it uncertain how migfilin-N would bind to IgFLNa21. We therefore set out to determine the solution structure of IgFLNc21 in complex with migfilin-N using a series of multidimensional heteronuclear NMR experiments. Fig. 3*B* shows the backbone superposition of 20 lowest energy NMR structures of the complex with a root mean square deviation of 0.3 Å for the backbone and 0.7 Å for all heavy atoms (see Table 1 for statistics). The overall fold of IgFLNc21 (Fig. 3*C*) is similar to the previously reported filamin Ig repeats, including IgFLNa17, IgFLNa21, IgFLNc23, and IgFLNc24 (16, 40–42). The backbone root mean square deviation between our NMR structure IgFLNc21 and the crystal structure of IgFLNa21 (16) is 1.6 Å. However, surprisingly, despite little sequence homology between migfilin-N and integrin β CTs (Fig. 3*A*), migfilin-N binds to exactly the same groove between β strands C and D in IgFLN21 (Fig. 3, *C* and *D*) where integrin β CTs bind (Fig. 3*E*). A total of 12 residues, Lys^{7}–Ala^{18}, of migfilin-N are involved in binding to IgFLN21, whereas in integrin β7, there is a 13-amino acid stretch sandwiched by two prolines that define the binding pocket. Migfilin lacks the N-terminal proline and has a lysine in its place (Fig. 3*A*). Structural inspection revealed that migfilin-N forms a β-sheet with strand C in IgFLNc21 (Fig. 3*C*) via conserved backbone hydrogen bonds as also seen in the integrin β7-IgFLNa21 complex. However, the side chain interactions appear to be very different between the two complexes

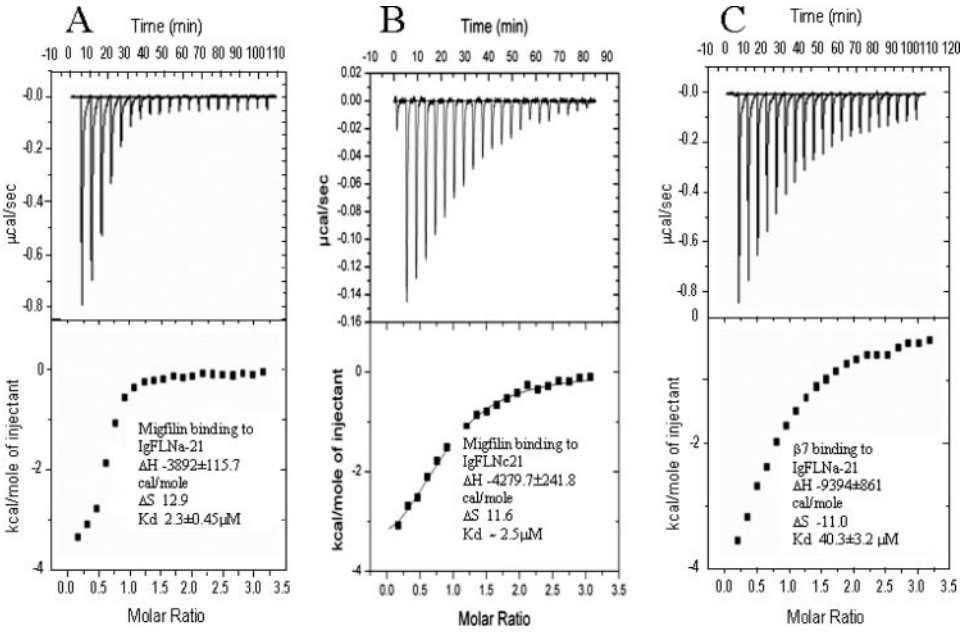

FIGURE 2. *A*, isothermal calorimetry data demonstrating similar migfilin binding of IgFLNa21; *B*, IgFLNc21. *C*, β7 binds IgFLNa21 at an order of magnitude lower affinity than migfilin.

TABLE 1

Structural statistics for the IgFLNc21-migfilin complex

r.m.s.d. indicates root mean square deviation.

Parameter	SA Ensemble
r.m.s.d. from experimental distance restraints (Å)	
All (1653)	
Intraresidue, $i = j$ (338)	0.0077 ± 0.001
Sequential, $\|i = j\| = 1$ (512)	0.0152 ± 0.002
Medium range, $1 < \|i = j\| < 5$ (219)	0.0325 ± 0.001
Long range, $\|i = j\| \geq 5$ (584)	0.0178 ± 0.001
Intermolecular, 130	
H-bonds, 38	
Dihedral angles, 80	
r.m.s.d. from idealized covalent geometry	
Bonds	0.0062 ± 0.0001 Å
Angles	0.9769 ± 0.0056
Impropers	1.5837 ± 0.0095
$E_{L\text{-}J}$	−383.012 ± 10 kcal/mol
Ramachandran plot	
Most favored regions	77.8%
Additionally and generously allowed regions	20.9%
Disallowed regions	1.2%
Coordinate precision	
r.m.s.d. of backbone atoms to the mean	0.30 Å
r.m.s.d. of all heavy atoms to the mean	0.70 Å

(Fig. 3, *F versus G*). Substantial hydrophobic interactions involving ^{9}V*XXX*VFI*X*L^{17} of migfilin-N are observed in the migfilin-N-IgFLNc21 complex (Fig. 3*G*). These hydrophobic residues are not conserved in integrin β CTs in which some of the corresponding positions are even occupied by hydrophilic residues (Fig. 3*A*). Hydrophobic residues Leu^{2327}, Ile^{2329}, Val^{2331}, Ile^{2339}, and Phe^{2341} on IgFLNc21 surround the migfilin Val^{13} and Ile^{15} side chains (Fig. 3*G*), whereas the corresponding positions in β7 are Ile^{782} and hydrophilic Thr^{784}, respectively (Fig. 3*F*). Phe^{14} in migfilin-N also makes hydrophobic contact with IgFLN21, whereas the corresponding Thr^{783} in β7 is hydrophilic. Thus, although the conserved backbone hydrogen bond pattern provides a basis for how migfilin-N and integrin β CTs recognize the same groove in IgFLNc21, the significantly more hydrophobic interactions in the migfilin-N-IgFLNc21 complex may explain why migfilin binds much tighter to IgFLNa21 than integrin β CTs. Among integrin β CTs, β7 has the closest hydrophobic match (Y*XXX*L*XXX*I) (Fig. 3*A*) to migfilin-N, ^{9}V*XXX*VFI*X*L^{17}, which may explain why integrin β7 is the tightest binder to IgFLN21 among integrin β CTs (16). During the submission of this manuscript, the crystal structure of IgFLNa21 in complex with migfilin-Pro^{5}–Pro^{19} was reported (see Ref. 43). Surprisingly, two IgFLNa21 molecules (chain A and chain B) were found to bind to one migfilin molecule because of possible crystallization effects. Although the backbone interactions were conserved in these two configurations, the side chain interactions were markedly different. Briefly, chain A interacted with the side chains of Ser^{11}, Val^{13}, and Ile^{15} of migfilin, whereas chain B interacted with those of Ser^{12}, Phe^{14}, and Thr^{16}. Our NMR structure clearly shows the IgFLNc21-migfilin-N interacts to form a 1:1 complex (based upon lack of increase in line widths), and the interface is very similar to the crystal structure of chain A/migfilin, thus resolving the uncertainty of the crystal structures. The chain B/migfilin structure is likely a crystallization artifact.

Migfilin-N Triggers Filamin-Integrin Dissociation, Promoting Talin-Integrin Interaction—The findings that migfilin-N and integrin β CT bind to the same site on IgFLN21 suggest that migfilin competes with integrin β CTs for binding to filamin. To experimentally test this hypothesis, we performed NMR-based competition experiments. Fig. 4*A* shows that although integrin β3 CT underwent significant chemical shift changes upon binding to IgFLNa21, no changes occurred when adding equivalent migfilin-N, demonstrating that the IgFLNa21 binding to integrin β3 CT was disrupted by the stronger IgFLNa21-migfilin-N interaction. Similarly, migfilin-N, which has much higher affinity for IgFLN21, displaced integrin β7 CT from binding to IgFLN21 (supplemental Fig. S4). This is consistent with the competition experiment reported by Lad *et al.* (43). NMR data also revealed that although IgFLNa21 blocks the integrin β CT binding to talin-PTB (Fig. 4*B*), consistent with previous co-immunoprecipitation data (16), migfilin-N can effectively remove the blocking effect of IgFLN21 and promote the talin-β CT interaction (Fig. 4*B*).

Migfilin Promotes Integrin Activation—Because the inhibition on talin-integrin β CT interaction by filamin negatively regulates integrin activation (16), the foregoing *in vitro* results led us to hypothesize that migfilin binding to filamin may positively regulate integrin activation by dissociating filamin from integrins. To functionally test this hypothesis, we first overexpressed migfilin in human melanoma, A7 cells (44), and examined binding of Alexa Fluor 647-labeled 120-kDa fibronectin

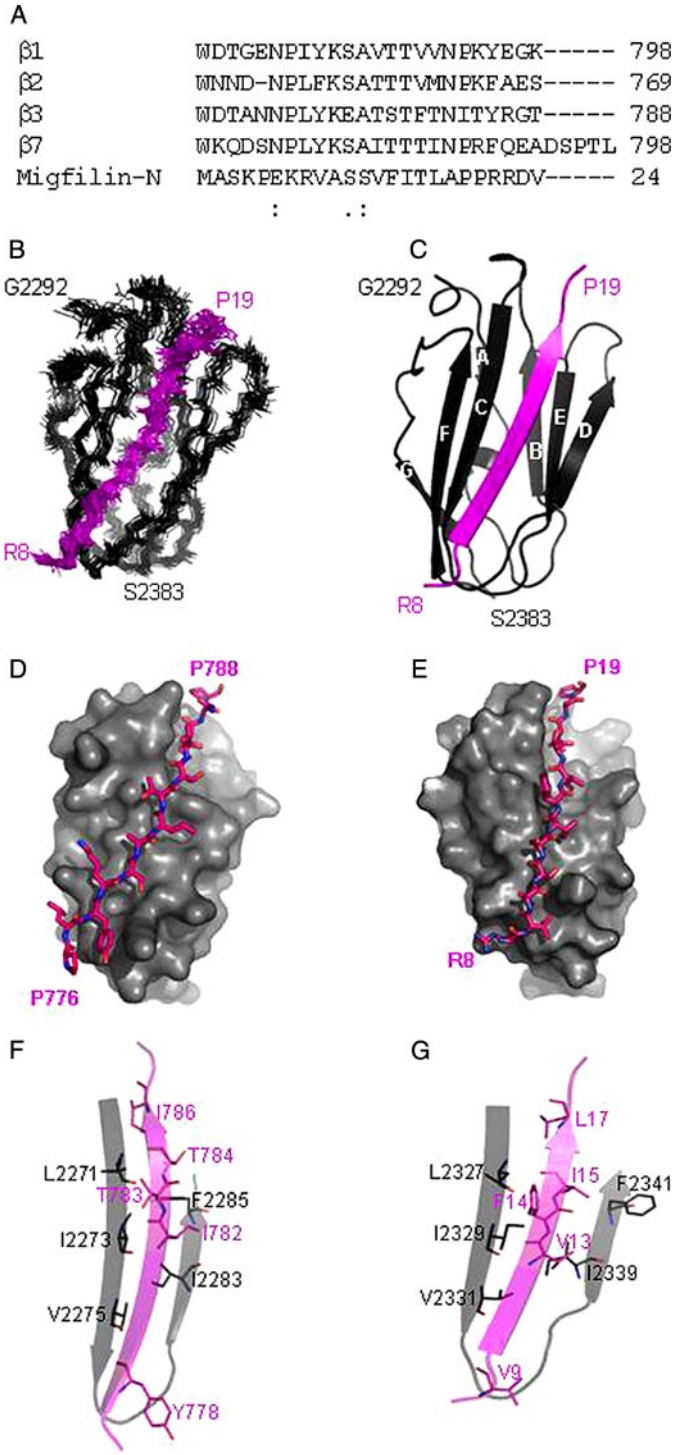

FIGURE 3. **Features of migfilin-N structure and its binding to IgFLN21.** *A,* sequence comparison of integrin β CTs and migfilin-N. *B,* backbone superposition of the 20 lowest energy NMR structures; and *C,* their corresponding ribbon representation (*right*). The bound migfilin-N is colored in *pink*, forming β-sheet with IgFLN21 strand C. *D,* surface depictions of IgFLNa21 bound to integrin β7 CT (PDB code 2brq). *E,* IgFLNc21 bound to migfilin-N. Comparison of *D* and *E* shows that β7 CT and migfilin-N bind to IgFLN21 in the same manner. *F,* detailed interface between IgFLNa21 and β7 CT (PDB code 2brq). *G,* detailed interface between IgFLNc21 and migfilin-N.

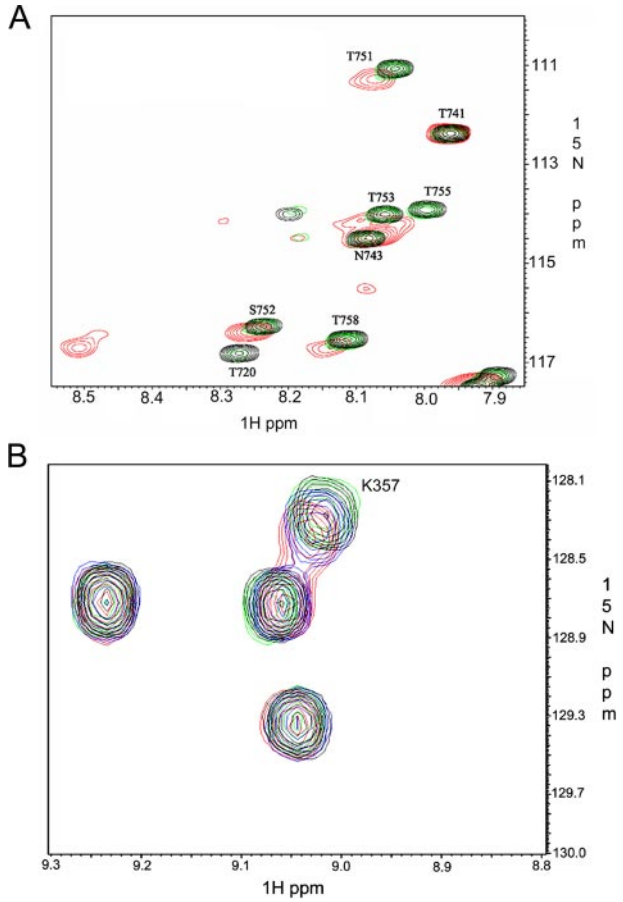

FIGURE 4. **Migfilin-N dissociates IgFLN21 from integrin β CTs and promotes talin-integrin interaction.** *A,* two-dimensional HSQC of 0.1 mM β3 CT (*black*) and β3 CT in the presence of 0.2 mM IgFLNc21 (*red*) and IgFLNc21/migfilin-N (1:2) (*green*), pH 5.6, 29 °C. The spectra in *red* and *green* are identical showing that migfilin-N-IgFLNc21 interaction prevented the IgFLN21 binding to β3 CT. *B,* HSQC spectra of a selected region of ^{15}N-labeled talin-PTB in the absence (*black*) and presence of unlabeled β7 CT (*red*) showing that talin-PTB interacts with β7 CT. The representative Lys^{357}, which is shifted upon addition of β7 CT, is known to be involved in interacting with integrin β CTs (14). Lys^{357} shifts back to the position of the free form talin-PTB (*green*) upon addition of IgFLNa21 demonstrating that the IgFLNa21 blocks the β7 CT binding to talin-PTB (talin-PTB:β7-CT:IgFLNa21 = 50:125:250 μM), but such blocking effect was significantly reduced (*blue*) upon addition of migfilin-N (talin-PTB:β7-CT:IgFLNa21:migfilin, *n* = 50:125:250:500 μM).

fragment, a ligand for β1 integrins, by FACS (45, 46). Western blots also confirmed the presence of the β1 subunit in these cells as reported previously (47). Fig. 5*A* shows that binding of the fibronectin fragment to A7 cells increased ~4-fold when the cells were transfected with vectors encoding for full-length migfilin as opposed to vector alone. Furthermore, binding of HUTS-4, a monoclonal antibody that reacts selectively with activated β1 integrins (48), also increased dramatically, demonstrating that overexpression of full-length migfilin enhances activation of integrins in these cells. These data provide the first line of functional evidence to support our model. Similar experiments were also attempted with the matched M2 melanoma cells, which lack filamin A (44). HUTS-4 binding to these cells transfected with either vector alone or with full-length migfilin was high suggesting high constitutive activation of the integrins in these cells.

To more definitively elucidate how the specific migfilin-filamin interaction regulates integrin activation, we explored a widely used model CHO cell line expressing integrin αIIbβ3 (A5 cells) and platelets that express high levels of this integrin. Full-length migfilin was expressed poorly in the CHO cells. Therefore, we chose an alternative approach and designed a

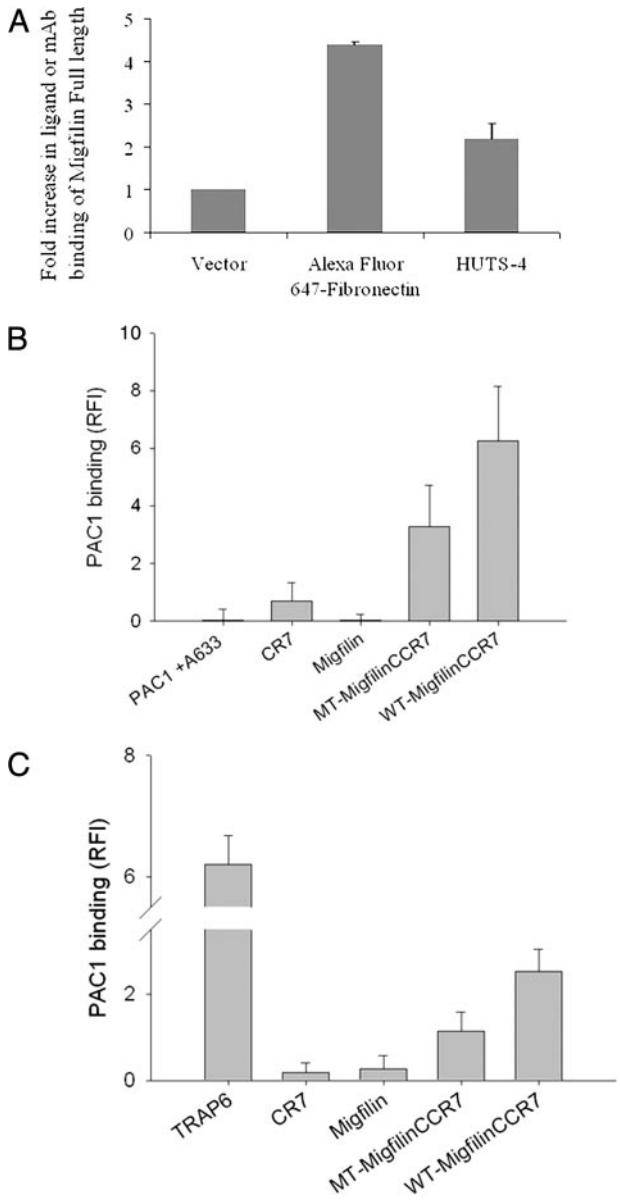

FIGURE 5. **Migfilin promotes integrin activation.** *A,* overexpression of migfilin promotes fibronectin and HUTS-4 (a mAb specific for the active conformation of the β1 integrin) binding of A7 melanoma cells. The cells were transfected with a vector encoding for GFP and full-length migfilin, and FACS were performed as described under "Experimental Procedures." The data shown are means ± S.E. for duplicate determinations, and the results are representative of 3–4 similar experiments. *B,* cell-deliverable migfilin-N (WT-MigfilinCCR7) enhances αIIbβ3 activation, as monitored with PAC-1, a mAb specific for the active conformation of this integrin. The cells used were CHO cells stably expressing αIIbβ3 (A5 cells). The mutant (MT-MigfilinCCR7) is significantly (p value <0.05) less effective in activating the integrin. The cell-permeable peptides, as well as the tag (CR7) and the untagged migfilin peptide, were added to the cells at 10 μM. After 5 min, the A5 cells were washed, and PAC-1 and an Alexa 633-conjugated secondary antibody were added. The cells were analyzed by FACS after an additional 30 min. *C,* cell-deliverable migfilin-N (WT-MigfilinCCR7) induces significant PAC1 binding to αIIbβ3 in platelets. In contrast, the filamin-binding defective migfilin-N mutant (MT-MigfilinCCR7) peptide had a significantly ($p < 0.05$) lower effect.

cell-deliverable peptide that contained only IgFLN21 binding sequence of migfilin conjugated to a hepta-Arg tag at the C terminus via a disulfide bond (termed CCR7) (see supplemental Fig. S4*A*). Compared with the full-length migfilin, this peptide, if effectively delivered to the cell, should only recognize filamin, which then would promote dissociation of filamin from integrin and talin-mediated integrin activation. The hepta-Arg tag (Arg^7) has been shown to be an efficient tool for peptide delivery into cells (34). The polyarginine tag by itself has minimal effects on cell function and morphology (49). Once the peptide enters the cell, the tag is cleaved by the more reducing intracellular environment thus minimizing nonspecific tag-protein interactions (34). Accordingly, we synthesized a peptide corresponding to residues Lys^4–Pro^{19} of migfilin with the CCR7 importer disulfide linked to its C terminus (WT-migfilin-CCR7, see supplemental Fig. S4*A*) and a mutant peptide (MT-migfilin-CCR7) in which two residues involved in filamin binding: Ser^{11} was replaced by Asp, and Val^{13} was replaced by Ala. This MT migfilin peptide binds at least 12.5 times weaker to IgFLNa21 than the WT peptide as assessed by NMR titration. These CCR7 peptides with a single FITC at their N terminus were incubated with platelets and A5 cells, and their uptake was monitored by fluorescence microscopy. The supplemental Fig. S5 shows that both the WT and MT CCR7 peptides successfully entered platelets. Two patterns were observed and are represented in the micrographs in supplemental Fig. S5, a punctate and a uniform fluorescent pattern. Similar patterns have been described in the literature of cells in which modified peptides have been taken up by cells (50, 51). Similar micrographs were also obtained with A5 cells stably expressing αIIbβ3 (not shown). We also found no uptake of the FITC-tagged migfilin peptide into the cells.

We first examined the peptide effect on the αIIbβ3 activation in A5 cells by using the activation-specific mAb PAC-1 as the first antibody and Alexa Fluor 633-labeled goat anti-mouse IgM as the second antibody to detect PAC-1 binding to the integrin as described previously (20, 52). Using the second antibody alone as background, the untreated A5 cells exhibited little reaction with PAC-1, consistent with the αIIbβ3 being in an unactivated state on these cells (see Fig. 5*B*). The untagged migfilin peptide and the tag itself had no effect on αIIbβ3 activation. In contrast, WT-migfilin-CCR7 activated the integrin. The MT-migfilin-CCR7 also induced PAC-1 binding, but it was significantly ($p < 0.05$) less potent than WT-migfilin-CCR7 (Fig. 5*B*). Thus, consistent with our hypothesis, the peptide corresponding to the filamin binding region of migfilin activated αIIbβ3, and mutations that reduced its filamin binding capacity reduced integrin activation. The differential effects of the WT- and MT-migfilin peptides were maintained over a wide range of peptide concentrations (supplemental Fig. S6).

Next, we sought to determine the αIIbβ3 activating activity of the migfilin peptides in platelets, the major blood cell expressing endogenous αIIbβ3. The activities of the migfilin peptides in platelets were found to be similar to those observed in the A5 cells, namely WT-migfilin-CCR7 induced extensive αIIbβ3 activation (Fig. 5*C*). At the concentration tested, it had ~50% of the activity of the positive control, the thrombin receptor activating peptide, TRAP. The MT-migfilin-CCR7 also induced αIIbβ3 activation, but it was significantly ($p <$ 0.05) less potent than WT-migifilin-CCR7. The control peptides, CR7 alone and the untagged migfilin peptide, had minimal activity (Fig. 5*C*).

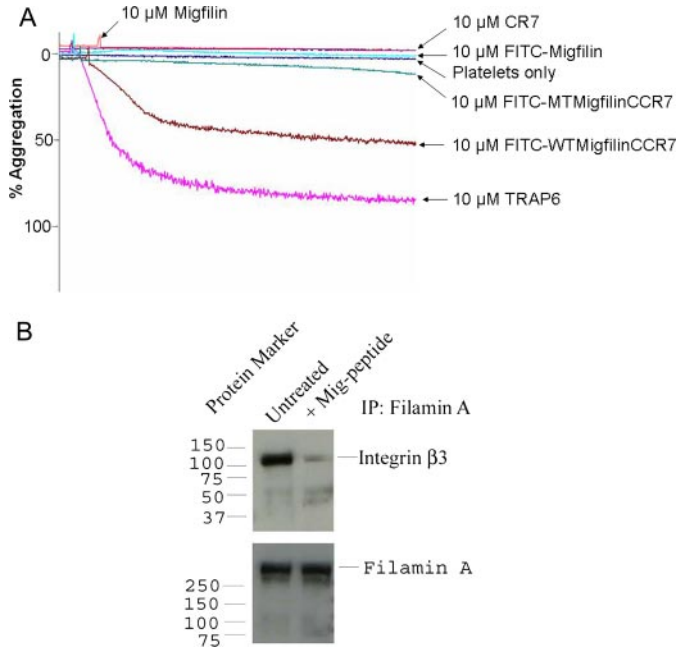

FIGURE 6. **Migfilin-N promotes platelet aggregation.** *A,* addition of WT-migfilin-CCR7 to a washed platelet suspension induced significant aggregation of the cells. This effect was minimal with the MT-migfilin-CCR7 at the same concentration and was not observed at all with the tag alone or the untagged WT-migfilin peptide. Data are representative of more than 10 experiments from at least five different donors. *B,* co-precipitation experiment showing that migfilin-N leads to dissociation of the filamin-integrin complex in platelet lysates. Data are representative of four independent experiments. *IP*, immunoprecipitation.

Further evidence for the functional activity of the WT-migfilin-CCR7 was obtained in platelet aggregation studies. As shown in Fig. 6*A*, addition of WT-migfilin-CCR7 to a washed platelet suspension induced significant aggregation of the cells, a response critically dependent upon the αIIbβ3 activation. This effect was minimal at the same concentration of the MT-migfilin-CCR7, and it was not observed at all with the tag alone or the untagged WT-migfilin peptide (see Fig. 6*A*). These differential effects of the WT and MT CR7 peptides on platelet aggregation were reproducible. Results shown in supplemental Fig. S7 are from three separate platelet preparations and are representative of data obtained with more than 10 different platelet preparations from at least five different donors. Peptides with or without the FITC label showed similar patterns of differential activities in platelet aggregation assays, although the CR7 with FITC tended to give a higher background aggregation than non-FITC labeled CR7. In control experiments, we found that the ADP-degrading enzyme, apyrase, at a concentration sufficient to block aggregation induced by 50 μM ADP, did not inhibit platelet aggregation induced by WT-migfilin-CCR7 (not shown). This latter result indicates that the effects of the peptides do not depend on the release of the agonist (ADP) either by induction of secretion or by lysis of some platelets.

To investigate if WT-migfilin-CCR7 peptide perturbed the filamin-integrin interaction in platelets, as predicted from our foregoing structural analyses, we performed co-immunoprecipitation experiments. Lysates from resting platelets were incubated with an antibody against filamin A, and co-precipitation of integrin β3 was detected by Western blotting with a mAb against the β3 subunit. Fig. 6*B* shows that although filamin A specifically associates with integrin β3 in platelets, consistent with previous biochemical analysis (53), this association was significantly reduced upon adding migfilin-N. As a control, similar amounts of filamin A were immunoprecipitated in the presence and absence of WT-migfilin-CCR7 (Fig. 6*B*, *lower panel*). Based on densitometric scans of these gels, the amount of β_3 immunoprecipitated in the presence of the WT-migfilin peptide was lowered by 55 $\pm$ 3% compared with the control (n = 4). These functional results thus strongly support the structure-based hypothesis that the binding of migfilin-N to filamin promotes integrin activation by dissociating the negative regulator filamin from integrins.

DISCUSSION

Dynamic regulation of integrin activation is important in many physiological cell adhesive events, including spreading, migration, and survival, and also influences pathological responses, such as tumor metastasis. Despite recent advances in unraveling the essential role of talin in activating integrins, the regulatory factor(s)/pathway(s) that control the activation process remain poorly defined. The extensive structural and functional data we have obtained here now suggest that migfilin binding to filamin provides at least one such regulatory pathway. Our evidence for involvement of this pathway has been obtained at both the structural and functional levels as follows. 1) Structurally, we showed that the N-terminal fragment of migfilin (migfilin-N) specifically binds to a region in filamin where integrin β CTs also bind and that such binding dissociates filamin from integrin and promotes the talin-integrin interaction. The structural data strongly suggest that migfilin-N may act as an off-switch for the filamin-integrin interaction that prevents talin binding and integrin activation. 2) Functionally, we showed the following: (i) Overexpression of migfilin significantly enhanced the integrin activation ~2–4-fold in A7 cells. (ii) Cell delivery of migfilin-N induced activation of a prototypic integrin αIIbβ3 in both a model cell system, A5 cells, and in a naturally occurring cell, platelets. (iii) Migfilin-N induced platelet aggregation, an event critically dependent upon the αIIbβ3 activation. In the peptide-based functional assays, a mutant migfilin peptide that has decreased affinity for filamin was substantially less effective in integrin activation. The decrease but not complete loss in the filamin binding activity of this migfilin mutant is consistent with its retention of some filamin binding activity (supplemental Fig. S4*B*). The nature of cell-permeable peptide uptake and resultant biological activities is yet to be resolved in the scientific literature (54).

How is migfilin localized to integrin adhesion sites to confer its regulatory function? Recent studies have identified a cytoskeletal protein kindlin-2/mig-2 that can efficiently recruit migfilin to cell-ECM adhesion sites (25). Kindlin-2 belongs to a family of kindlin proteins (kindlin-1, -2, and -3) that are highly homologous and contain talin-like FERM domains. Remarkably, both kindlin-2 and kindlin-3 have been shown to be also involved in regulating talin-mediated integrin activation (19–20, 55–56). Kindlin-2 and talin were shown to bind to different regions of membrane-distal β_3 CT and act synergistically in inducing integrin activation (20, 56). The kindlin-2 function has

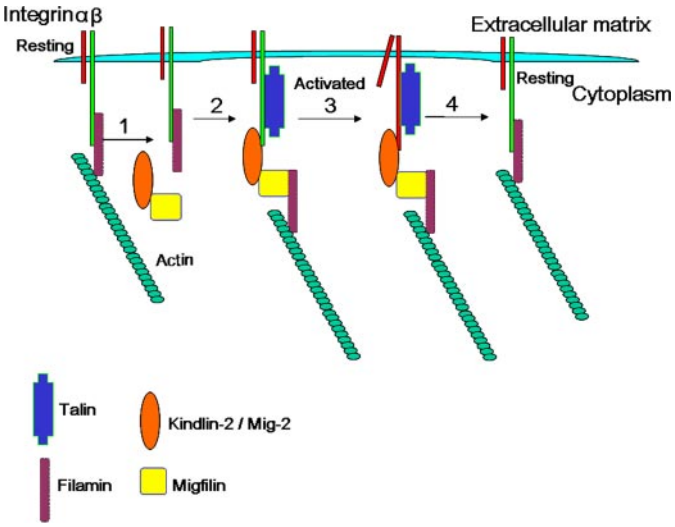

FIGURE 7. **A model for the role of the migfilin-filamin interaction in regulating integrin activation and cytoskeleton reassembly.** Migfilin is recruited by kindlin-2 (*Mig-2*) to integrin adhesion sites (25). The recruited migfilin promotes dissociation of filamin from integrins, which is bound to the resting integrin and inhibits the talin-integrin interaction (16) as well as the anchoring of kindlins to integrin β CTs. When filamin is displaced, talin and kindlins become more effective in mediating integrin activation. Because filamin is a major actin cross-linking protein critical for maintaining the actin network, the migfilin-induced disconnection between integrin and filamin may also cause temporal rearrangement of the integrin-actin linkage to facilitate the cytoskeleton remodeling.

been shown to be dependent upon its interaction with migfilin as deletion of N-terminal kindlin-2 critical for binding to migfilin (25) abolished the kindlin-2 effect on integrin activation (20) and dramatically impaired localization of migfilin to integrin containing focal adhesion sites and cell spreading (25). Thus, filamin, migfilin, and kindlin(s) may constitute a unit within the multiprotein machinery for cooperative regulation of integrin activation. Accordingly, migfilin may play a dual role in this pathway (Fig. 7) as follows: (i) Binding filamin via its N terminus to promote the dissociation of inhibitory filamin from integrins thereby facilitating the talin-integrin interaction. (ii) Binding kindlin-2 or -3 via its C-terminal LIM domain (25) to promote the anchoring of kindlin-2/3 to integrin β3 CT and to further strengthen the talin effect as a co-factor for integrin activation. It should be noted that because filamin is a major actin cross-linking protein and is critical for maintaining the actin network, the migfilin-induced disconnection between integrin and filamin not only facilitates the talin-mediated integrin activation but also may cause temporal rearrangement of the integrin-actin linkage to facilitate the cytoskeleton remodeling. This model is supported by previous unexplained functional data that showed that specific disruption of the filamin-migfilin interaction by deleting migfilin-N impaired actin assembly (25). However, migfilin is not an evolutionarily conserved protein in multicellular animals, being absent in *Drosophila*. It is therefore possible that migfilin and modulation by migfilin(s) of integrin activity are superimposed on a more fundamental activation cascade. Cell type and cellular metabolic status may determine the outcome of interventions like overexpression and protein uptake studies.

In summary, we have identified a novel migfilin/filamin-mediated pathway for regulating integrin activation. Our combined structural and functional data provide compelling evidence that the binding of migfilin to filamin disconnects the inhibitory filamin from integrins thereby promoting the efficient talin binding to and activation of the receptors and the reorganization of the actin cytoskeleton. In light of the central importance of the talin and its role in integrin activation in various pathological processes, our findings, especially the cell-delivery peptides, may lead to the design of better compounds to repair dysfunction of integrin-mediated adhesive processes. These peptides may also provide valuable means to examine integrin signaling and cell adhesion in diverse biological processes.

Acknowledgments—We thank Yizhuang Xu and Jun Yang for help with assignments and scripts; Saurav Misra for advice on ITC; Xiaolun Zhang for help with figures; Esen Goksey for talin head domain; and Xi-An Mao, Jianmin Liu, and Julia Vaynberg for assistance and useful discussions.

REFERENCES

1. Hynes, R. O. (2002) *Cell* **110,** 673–687
2. Qin, J., Vinogradova, O., and Plow, E. F. (2004) *PLoS Biol.* **2,** e169
3. Arnaout, M. A., Goodman, S. L., and Xiong, J. P. (2007) *Curr. Opin. Cell Biol.* **19,** 495–507
4. Luo, B. H., Carman, C. V., and Springer, T. A. (2007) *Annu. Rev. Immunol.* **25,** 619–647
5. Ma, Y. Q., Qin, J., and Plow, E. F. (2007) *J. Thromb. Haemost.* **5,** 1345–1352
6. Hughes, P. E., Diaz-Gonzalez, F., Leong, L., Wu, C., McDonald, J. A., Shattil, S. J., and Ginsberg, M. H. (1996) *J. Biol. Chem.* **271,** 6571–6574
7. Vinogradova, O., Velyvis, A., Velyviene, A., Hu, B., Haas, T., Plow, E., and Qin, J. (2002) *Cell* **110,** 587–597
8. Kim, M., Carman, C. V., and Springer, T. A. (2003) *Science* **301,** 1720–1725
9. Ma, Y. Q., Yang, J., Pesho, M. M., Vinogradova, O., Qin, J., and Plow, E. F. (2006) *Biochemistry* **45,** 6656–6662
10. Takagi, J., Petre, B. M., Walz, T., and Springer, T. A. (2002) *Cell* **110,** 599–611
11. Luo, B. H., Springer, T. A., and Takagi, J. A. (2004) *PLoS Biol.* **2,** e153
12. Partridge, A. W., Liu, S., Kim, S., Bowie, J. U., and Ginsberg, M. H. (2005) *J. Biol. Chem.* **280,** 7294–7300
13. Li, W., Metcalf, D. G., Gorelik, R., Li, R., Mitra, N., Nanda, V., Law, P. B., Lear, J. D., Degrado, W. F., and Bennett, J. S. (2005) *Proc. Natl. Acad. Sci. U. S. A.* **102,** 1424–1429
14. Wegener, K. L., Partridge, A. W., Han, J., Pickford, A. R., Liddington, R. C., Ginsberg, M. H., and Campbell, I. D. (2007) *Cell* **128,** 171–182
15. Martel, V., Racaud-Sultan, C., Dupe, S., Marie, C., Paulhe, F., Galmiche, A., Block, M. R., and Albiges-Rizo, C. (2001) *J. Biol. Chem.* **276,** 21217–21227
16. Kiema, T., Lad, Y., Jiang, P., Oxley, C. L., Baldassarre, M., Wegener, K. L., Campbell, I. D., Ylänne, J., and Calderwood, D. A. (2006) *Mol. Cell* **21,** 337–347
17. Han, J., Lim, C. J., Watanabe, N., Soriani, A., Ratnikov, B., Calderwood, D. A., Puzon-McLaughlin, W., Lafuente, E. M., Boussiotis, V. A., Shattil, S. J., and Ginsberg, M. H. (2006) *Curr. Biol.* **16,** 1796–1806
18. Millon-Frémillon, A., Bouvard, D., Grichine, A., Manet-Dupé, S., Block, M. R., and Albiges-Rizo, C. (2008) *J. Cell Biol.* **180,** 427–441
19. Moser, M., Nieswandt, B., Ussar, S., Pozgajova, M., and Fässler, R. (2008) *Nat. Med.* **14,** 325–330
20. Ma, Y. Q., Qin, J., Wu, C., and Plow, E. F. (2008) *J. Cell Biol.* **181,** 439–446
21. Stossel, T. P., Condeelis, J., Cooley, L., Hartwig, J. H., Noegel, A., Schleicher, M., and Shapiro, S. S. (2001) *Nat. Rev. Mol. Cell Biol.* **2,** 138–145
22. Feng, Y., and Walsh, C. A. (2004) *Nat. Cell Biol.* **6,** 1034–1038
23. Takala, H., Nurminen, E., Nurmi, S. M., Aatonen, M., Strandin, T., Takatalo, M., Kiema, T., Gahmberg, C. G., Ylanne, J., and Fagerholm, S. C.

(2008) *Blood* **112,** 1853–1862
24. Calderwood, D. A., Huttenlocher, A., Kiosses, W. B., Rose, D. M., Woodside, D. G., Schwartz, M. A., and Ginsberg, M. H. (2001) *Nat. Cell Biol.* **3,** 1060–1068
25. Tu, Y., Wu, S., Shi, X., Chen, K., and Wu, C. (2003) *Cell* **113,** 37–47
26. Zhang, Y., Tu, Y., Gkretsi, V., and Wu, C. (2006) *J. Biol. Chem.* **281,** 12397–12407
27. Delaglio, F., Grzesiek, S., Vuister, G. W., Zhu, G., Pfeifer, J., and Bax, A. (1995) *J. Biomol. NMR* **6,** 277–293
28. Garrett, D. S., Powers, R., Gronenborn, A. M., and Clore, G. M. (1991) *J. Magn. Reson.* **95,** 214–220
29. Xu, Y., Wang, X., Yang, J., Vaynberg, J., and Qin, J. (2006) *J. Biomol. NMR* **34,** 41–56
30. Schwieters, C. D., Kuszewski, J. J., Tjandra, N., and Clore, G. M. (2003). *J. Magn. Reson.* **160,** 65–73
31. Cornilescu, G., Delaglio, F., and Bax, A. (1999) *J. Biomol. NMR* **13,** 289–302
32. Laskowski, R. A., MacArthur, M. W., Moss, D. S., and Thornton, J. M. (1993) *J. Appl. Crystallogr.* **26,** 283–291
33. Ugarova, T. P., Budzynskiv, A. Z., Shattil, S. J., Ruggeri, Z. M., Ginsberg, M. H., and Plow, E. F. (1993) *J. Biol. Chem.* **268,** 21080–21087
34. Chen, L., Wright, L. R., Chen, C. H., Oliver, S. F., Wender, P. A., and Mochly-Rosen, D. (2001) *Chem. Biol.* **8,** 1123–1129
35. Cunningham, C. C., Gorlin, J. B., Kwiatkowski, D. J., Hartwig, J. H., Janmey, P. A., Byers, H. R., and Stossel, T. P. (1992) *Science* **255,** 325–327
36. Martin, K., Meade, G., Moran, N., Shields, D. C., and Kenny, D. (2003) *J. Thromb. Haemost.* **1,** 2643–2652
37. Akazawa, H., Kudoh, S., Mochizuki, N., Takekoshi, N., Takano, H., Nagai, T., and Komuro, I. A. (2004) *J. Cell Biol.* **164,** 395–405
38. Takafuta, T., Saeki, M., Fujimoto, T. T., Fujimura, K., and Shapiro, S. S. (2003) *J. Biol. Chem.* **278,** 12175–12181
39. Wu, C. (2005) *J. Cell Sci.* **118,** 659–664
40. Pudas, R., Kiema, T. R., Butler, P. J., Stewart, M., and Ylänne, J. (2005) *Structure* (*Lond.*) **13,** 111–119
41. Nakamura, F., Pudas, R., Heikkinen, O., Permi, P., Kilpeläinen, I., Munday, A. D., Hartwig, J. H., Stossel, T. P., and Ylänne, J. (2005) *Blood* **107,** 1925–1932
42. Sjekloća, L., Pudas, R., Sjöblom, B., Konarev, P., Carugo, O., Rybin, V., Kiema, T. R., Svergun, D., Ylänne, J., and Djinović Carugo, K. (2007) *J. Mol. Biol.* **368,** 1011–1023
43. Lad, Y., Jiang, P., Ruskamo, S., Harburger, D. S., Ylänne, J., Campbell, I. D., and Calderwood, D. A. (2008) *J. Biol. Chem.* **283,** 35154–35163
44. Flanagan, L. A., Chou, J., Falet, H., Neujahr, R., Hartwig, J. H., and Stossel, T. P. (2001) *J. Cell Biol.* **155,** 511–517
45. Zhang, Z., Morla, A. O., Vuori, K., Bauer, J. S., Juliano, R. L., and Ruoslahti, E. (1993) *J. Cell Biol.* **122,** 235–242
46. Faull, R. J., Kovach, N. L., Harlan, J. M., and Ginsberg, M. H. (1993) *J. Cell Biol.* **121,** 155–162
47. Klaile, E., Muller, M. M., Kannicht, C., Singer, B. B., and Lucka, L. (2005). *J. Cell Sci.* **116,** 5513–5524
48. Luque, A., Go′mez, M., Puzon, W., Takada, Y., Sánchez-Madrid, F., and Cabañas, C. (1996) *J. Biol. Chem.* **271,** 11066–11075
49. David, T., Ohlmann, P., Eckly, A., Moog, S., Cazenave, J. P., Gachet, C., and Lanza, F. (2006) *J. Thromb. Haemost.* **4,** 2645–2655
50. Nelson, A. R., Borland, L., Allbritton, N. L., and Sims, C. E. (2007) *Biochemistry* **46,** 14771–14781
51. Ye, Y., Bloch, S., Xu, B., and Achilefu, S. (2006) *J. Med. Chem.* **49,** 2268–2275
52. Watanabe, N., Bodin, L., Pandey, M., Krause, M., Coughlin, S., Boussiotis, V. A., Ginsberg, M. H., and Shattil, S. J. (2008) *J. Cell Biol.* **181,** 1211–1222
53. Goldmann, W. H. (2000) *Biochem. Biophys. Res. Commun.* **271,** 553–557
54. Trehin, R., and Merkle, H. P. (2004) *Eur. J. Pharm. Biopharm.* **58,** 209–223
55. Shi, X., Ma, Y. Q., Tu, Y., Chen, K., Wu, S., Fukuda, K., Qin, J., Plow, E. F., and Wu, C. (2007) *J. Biol. Chem.* **282,** 20455–20466
56. Montanez, E., Ussar, S., Schifferer, M., Bösl, M., Zent, R., Moser, M., and Fässler, R. (2008) *Genes Dev.* **22,** 1325–1330